Journal of Advanced Research in
Applied Mechanics

Journal homepage:
https://semarakilmu.com.my/journals/index.php/appl_mech/index
ISSN: 2289-7895

Forecasting the Critical Frequency of the Ionospheric F2 Layer by using a Neural Network with the Particle Swarm Optimization Algorithm

Mariyam Jamilah Homam[1,*], Noreen Nabilla Risal[1], Rohaida Mat Akir[1], Suryadi Suryadi[2]

[1] Department of Electronic Engineering, Faculty of Electrical and Electronic Engineering, Parit Raja, 86400 Batu Pahat, Johor, Malaysia
[2] Department of Electrical Engineering, Politeknik Negeri Padang, Kota Padang, Sumatera Barat 25164, Indonesia

ARTICLE INFO

Article history:
Received 17 September 2024
Received in revised form 19 October 2024
Accepted 25 October 2024
Available online 30 November 2024

Keywords:
Critical frequency; ionosphere; backpropagation neural network; particle swarm optimization

ABSTRACT

This paper considers the prediction of the critical frequencies of the ionospheric F2 layer, f_oF_2, by using two models: a backpropagation neural network (BPNN) model and a BPNN combined with particle swarm optimization (BPNN–PSO) model for different states of solar activity: low, medium and high. Nine-year critical frequency data from an ionosonde installed at the Universiti Tun Hussein Onn Malaysia in Johor (1.86° N, 103.80° E) were used. The efficiency of the models in predicting f_oF_2 under different states of solar activity was explored. The output of the models was evaluated using root-mean-square error (RMSE) and mean average percentage error (MAPE). The BPNN–PSO model provided a better result compared with the BPNN model during low, medium and high solar activity. The BPNN–PSO model had RMSE and MAPE equal to 0.50 MHz and 5.27%, respectively, during low solar activity and RMSE and MAPE of 0.32 MHz and 4.16%, respectively, during medium solar activity. In addition, the BPNN–PSO model had the lowest RMSE (0.24 MHz) and MAPE (2.45%) during high solar activity. Overall, the performance of the BPNN–PSO model was higher than that of the BPNN model during any state of solar activity.

1. Introduction

Variability in ionospheric parameters depends on space weather disturbances that affect the efficiency of communication, radar and navigation systems. One of the most important ionospheric parameters is the critical frequency of the ionospheric F2 layer, f_oF_2. This value depends on local time, geographical latitude, solar and geomagnetic activity, wind from the atmosphere and other factors [1]. This value is crucial for forecasting high-frequency (HF) communication [2]. HF radio signals are well known for frequently enabling low-cost long-distance communication 24 hours a day [3]. Consequently, f_oF_2 must be predicted by considering factors of the instability of the ionosphere, limiting the capability for achieving accurate frequencies for HF communication.

f_oF_2 has been predicted using a variety of techniques. Researchers, such as Wang *et al.,* [4] and Pietrella [5], created analytical models to predict the changes of f_oF_2. A backpropagation neural

---

[*] *Corresponding author.*
E-mail address: mariyam@uthm.edu.my

https://doi.org/10.37934/aram.127.1.1629

network (BPNN), rather than an empirical model, was used in several studies to test the outcomes [6-11]. Ionospheric parameters perform better when they are predicted using BPNN than when using an empirical model. Nonetheless, this technique has major disadvantages, such as a slow convergence rate and a propensity to end up in local minima [2]. The inherent flaws in the current algorithm were addressed by utilizing a convolutional neural network [12], genetic algorithm (GA) [1,9], particle swarm optimization (PSO) [2,13,14], AdaBoost-BP algorithm [15] and the empirical orthogonal function model [16].

Based on data from 2004 to 2012, this paper develops a single-station neural network model for forecasting the value of f_oF_2 near the Universiti Tun Hussein Onn Malaysia (UTHM). This paper examines the performance of the developed f_oF_2 forecasting model under various states of solar activity by using BPNN and BPNN combined with PSO (BPNN–PSO). Other works have shown that PSO can provide better outcomes in forecasting. Therefore, it is employed in our work in forecasting the critical frequency of the ionospheric F2 layer.

2. Methodology

Ionospheric variability depends on local time, latitude, solar and geomagnetic activities and other factors [17-20]. The input parameters of the f_oF_2 model are diurnal and seasonal variations, solar activity, solar flux and sunspot number. The proposed networks were developed using nine-year ionogram data collected from the Canadian Advanced Digital Ionosonde (CADI) at the Advanced Telecommunication Research Centre (formerly known as Wireless and Radio Science Centre), UTHM. Two different methods, namely, general BPNN and BPNN with PSO, were used to forecast the value of the critical frequency.

2.1 Inputs to the Prediction Models

Eight input parameters were used related to day number (DN), universal time (UT), sunspot number (SSN), solar flux F10.7, global geomagnetic index K_p and equatorial geomagnetic index D_{st}. These parameters represent diurnal and seasonal variations and solar and geomagnetic variations.

2.1.1 Diurnal and seasonal variations

Diurnal and seasonal variations were represented by a UT of 0000 to 2300 and a DN of 1 to 365. Based on the previous work, the sine and cosine of UT and DN were translated into quadrative components in Eq. (1) to Eq. (4) [2].

$$UTS = \sin\left(\frac{2\pi \times UT}{24}\right) \tag{1}$$

$$UTC = \cos\left(\frac{2\pi \times UT}{24}\right) \tag{2}$$

$$DNS = \sin\left(\frac{2\pi \times DN}{365}\right) \tag{3}$$

$$DNC = \cos\left(\frac{2\pi \times DN}{365}\right) \tag{4}$$

2.1.2 Solar variations

The SSN and solar flux F10.7 obtained from the NASA/Goddard Space Flight Centre Physics Data Facility were used as input parameters to indicate solar activity. The values can be grouped into three phases: low, medium and high solar levels of activity. Table 1 and Figure 1 present the yearly mean of SSN dan solar flux F10.7 and the daily SSN dan solar flux, respectively, from January 2004 to December 2012, which covers all three solar activity phases.

Table 1
Yearly mean of SSN and solar flux F10.7 from January to December (2004 to 2012)

Year	Mean SSN	Mean Solar Flux F10.7	Solar Activity Level
2004	65.34	106.49	High
2005	45.71	91.71	Medium
2006	24.67	79.99	Medium
2007	12.64	73.07	Low
2008	4.15	74.16	Low
2009	4.76	70.54	Low
2010	24.90	79.99	Medium
2011	80.81	115.70	High
2012	84.39	122.29	High

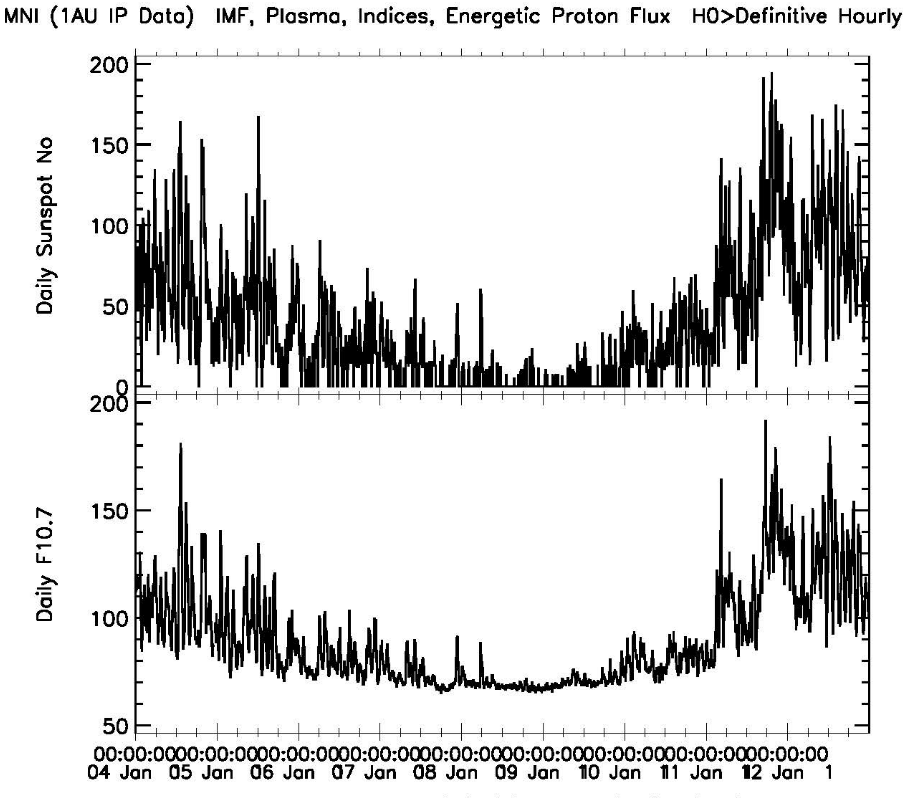

Fig. 1. Daily sunspot number and solar flux F10.7 data from January 2004 to December 2012 [21]

2.1.3 Geomagnetic variations

A geomagnetic storm is a substantial disturbance of Earth's magnetosphere caused by an intense energy flux from the solar wind into the planet's surroundings [17]. f_oF_2 varies dramatically in accordance with solar and geomagnetic activities. Geomagnetic indices, such as K_p and D_{st}, reflect geomagnetic storm activities.

This neural network modelling technique was used to predict f_oF_2 values under quiet and disturbed conditions. Thus, geomagnetic storm parameters K_p and D_{st} were used to represent a geomagnetic storm activity. Table 2 provides the equatorial geomagnetic disturbance level, D_{st}.

Table 2
Equatorial geomagnetic disturbance level, D_{st}

Geomagnetic disturbance level	Peak D_{st} (nT)
Quiet condition	Peak $D_{st} > -20$
Weak storm	Peak $D_{st} > -50$
Moderate storm	$-100 < Peak\ D_{st} < -50$
Intense storm	Peak $D_{st} < -100$

Table 3 presents the level of global geomagnetic disturbance level, K_p, along with its equivalent value.

Table 3
Global geomagnetic disturbance level, K_p

Geomagnetic disturbance level	K_p index	Equivalent K_p index
Quiet condition	0–4	3–43
Weak storm	5	47–53
Moderate storm	6–7	57–73
Intense storm	8–9	77–93

Figure 2 shows the three-hour K_p and one-hour D_{st} data obtained from CDAWeb for the whole period of the training and testing data, which covers all geomagnetic conditions: quiet and storm.

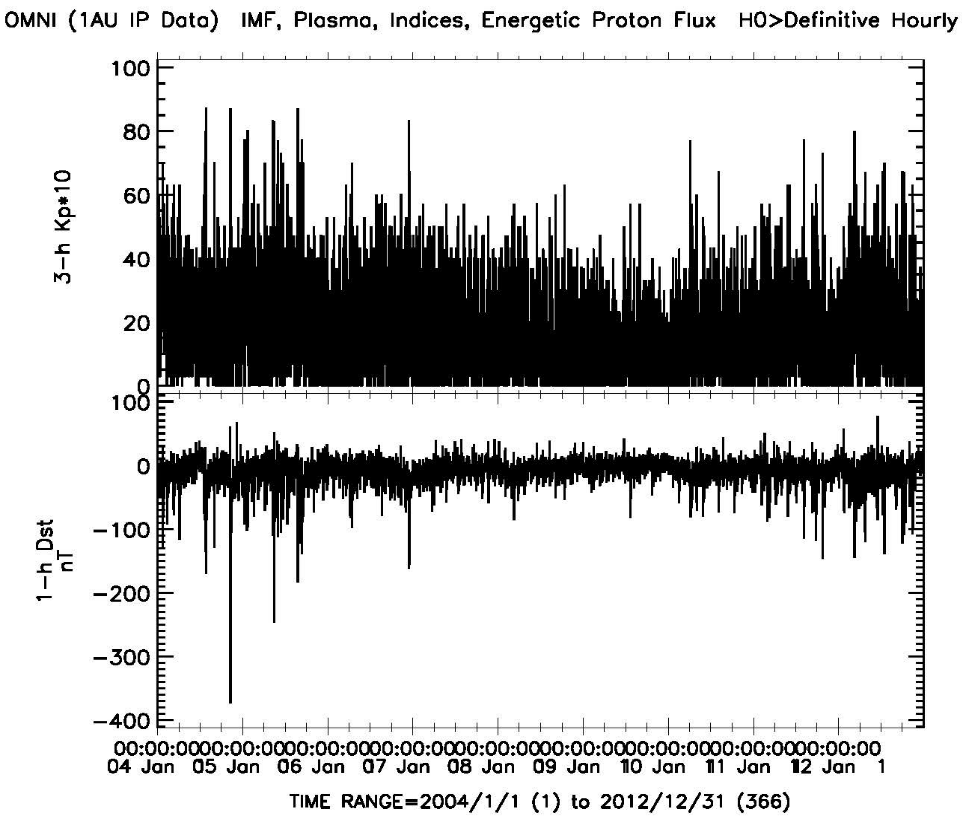

Fig. 2. 3-hour K_p and 1-hour D_{st} data from January 2004 to December 2012 [21]

2.2 Outputs of the Prediction Models

This paper examined the association between the actual and predicted values of f_oF_2 by using the ionogram data obtained from the CADI ionosonde at UTHM. Figure 3 illustrates an example of CADI's ionogram showing the reflection signal from the F2 layer on 23 December 2004. The value of f_oF_2 was manually extracted from the ionogram.

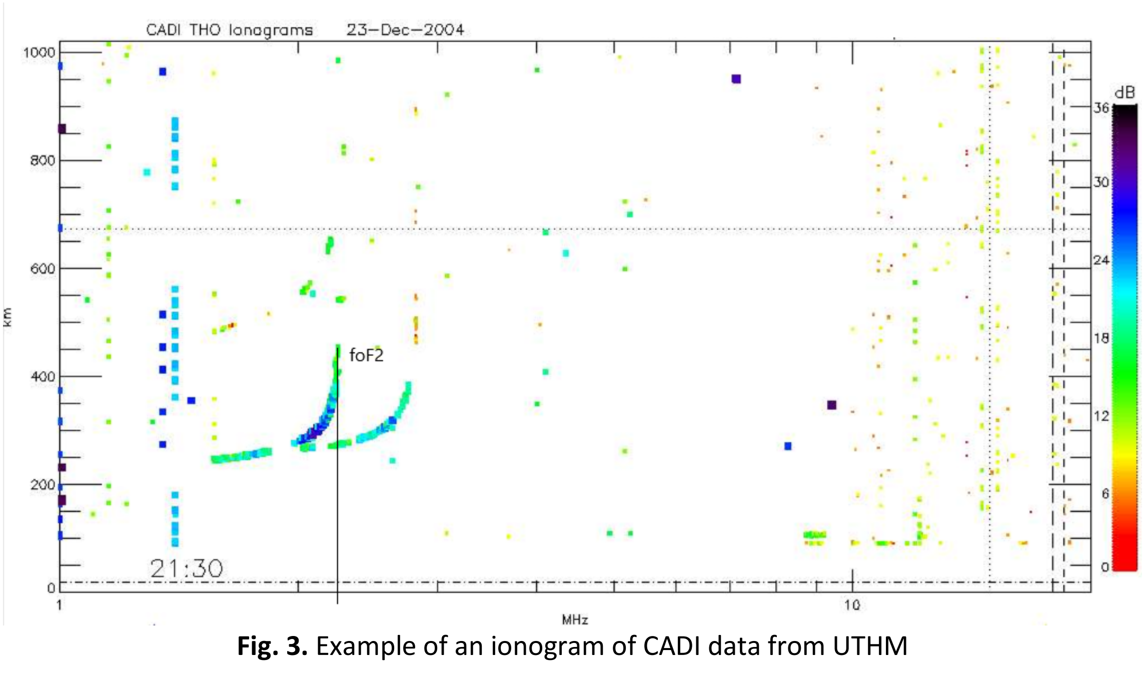

Fig. 3. Example of an ionogram of CADI data from UTHM

2.3 f_oF_2 Prediction Model using BPNN

Figure 4 presents the BPNN topology used in this work with eight inputs and one output. The BPNN employed two hidden layers. The number of hidden neurons was determined based on a few trials that fulfilled the training stopping criteria.

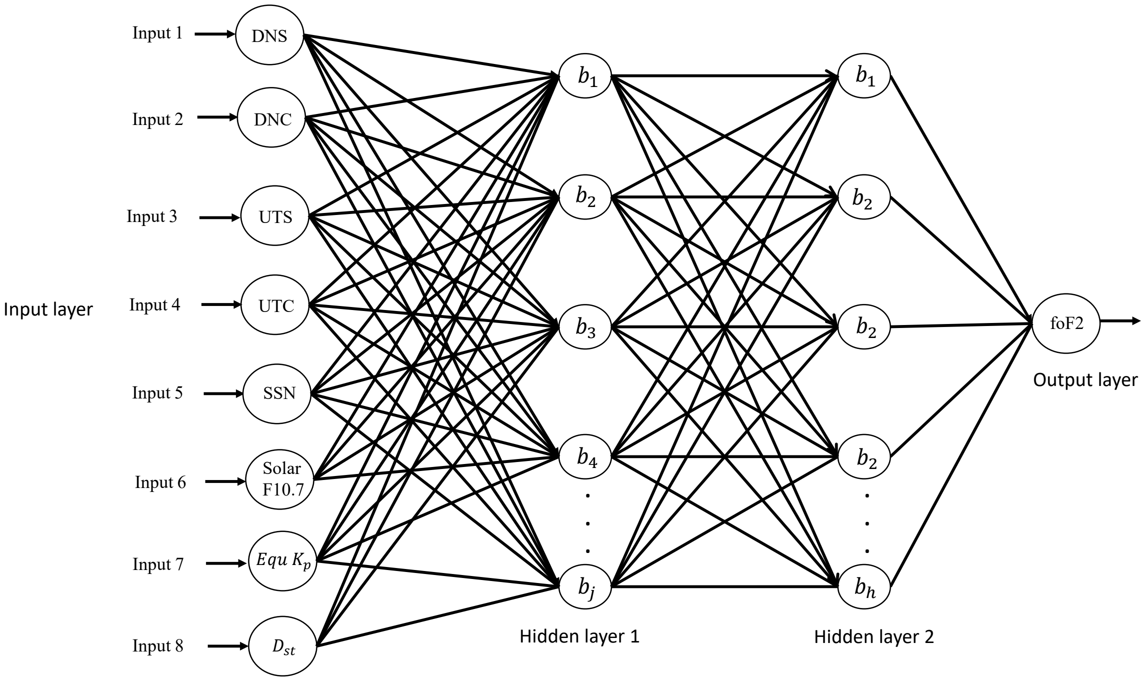

Fig. 4. BPNN topology

2.4 f_oF_2 Prediction Model Optimized using PSO

PSO is a computational method that describes the movement of organisms in a flock of birds or a school of fish as simplified and optimized by the algorithm. In PSO, each particle can learn from the others' outcomes, enabling it to use all available data [13]. Figure 5 illustrates the flowchart of BPNN–PSO. The position is represented by P(m) and each particle moves at a velocity of V(m). Each part in the swarm is randomly driven by a controlled parameter that will be addressed later. After each particle movement, the particle evaluates it's fitting value with the previous best value that the particle has achieved so far. If the current fitness value is better than the previous value, the particle position is recorded as a P_{best}. A global best value is achieved by comparing all particles' fitness values, selecting the best value between them and comparing them with the previous global best value. If the previous global best value is lower than the current global best value, the global best value is recorded with its position and this new position represents a global best position as G_{best}.

Particle movement is controlled by three parameters: inertia weight (i_w), local acceleration constant (C_1) and global acceleration constant (C_2). Inertia weight is used to monitor the contribution of the past particle velocity to the current particle velocity. Local acceleration constant (C_1) is used to monitor the velocity's contribution due to the difference between the current part position. Due to the difference between current particle position and global best position, particle best position and global acceleration constant (C_2) are used to monitor velocity contribution. The fitness function value for each particle is calculated.

Then, the position of the particle whose fitness function value is the smallest is chosen as the local minimum (P_{best}) and the global minimum (G_{best}). Each particle's velocity and position are updated using the known local and global best. The next step is verifying the stop conditions have been met. If yes, it is then stopped and the latest global best is selected as input for the neural network system. Otherwise, all steps from measuring fitness values are repeated until a new stop is achieved.

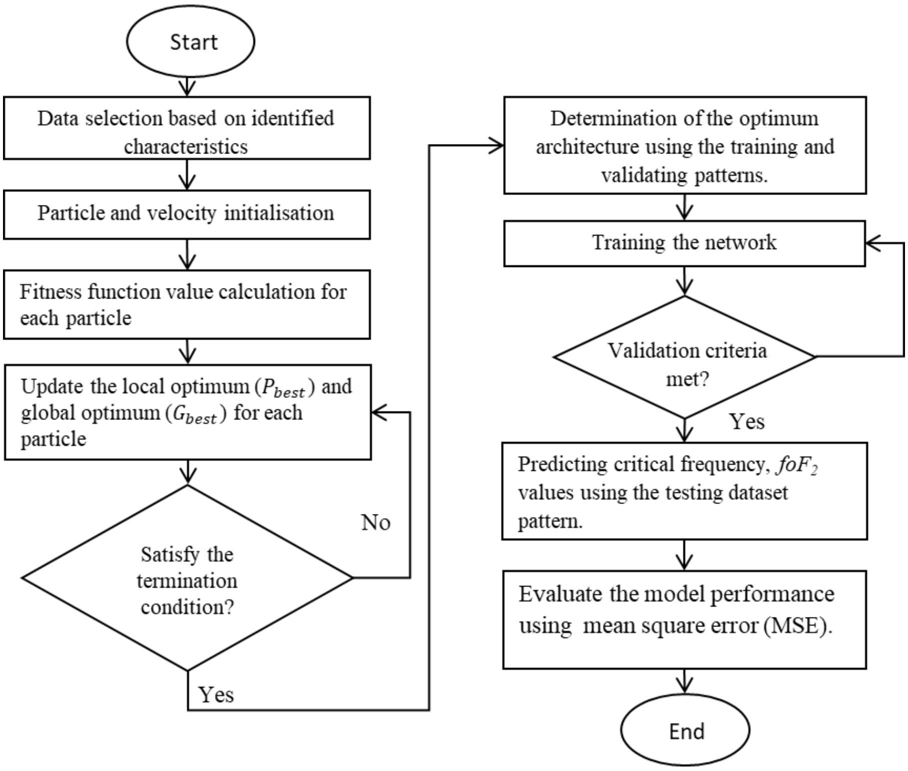

Fig. 5. Flowchart of BPNN–PSO

2.5 Training, Validation and Testing Phases
2.5.1 Datasets

The processed ionogram data were split into two sets: training and testing datasets. Several network properties were modified to construct the optimum BPNN model. Training was performed using feedforward backpropagation and the Levenberg–Marquardt algorithm (TRAINLM). Table 4 provides the input ranges of the training dataset, which covers all three phases of solar activity, namely, low, medium and high and quiet and disturbed geomagnetic activity.

Table 4
Input ranges of the training dataset

Model	BPNN and BPNN–PSO
SSN	0–167
Solar flux F10.7	70.7–170.4
Equivalent K_p index	0–87
D_{st} index (nT)	−320–30

Table 5 shows the training parameters for the BPNN and BPNN–PSO models to predict f_oF_2. All training parameters are the same for both models, except for the numbers of hidden neurons, namely, 13 for the BPNN model and 11 for BPPNN–PSO. These numbers were chosen because they resulted in the optimum training outcomes.

Table 5
Training parameters for BPNN and BPNN–PSO

Parameter	BPNN	BPNN–PSO
Number of training data	10500	10500
Number of hidden layers	2	2
Number of hidden neurons	13	11
Training function	TRAINLM	TRAINLM
Adaption learning function	LEARNGDM	LEARNGDM
Transfer function	TANSIG	TANSIG
Performance function	MSE	MSE

Table 6 presents the selected testing datasets to compare the performance of the BPNN and BPNN–PSO models during different solar activities and their monthly mean SSN and solar flux F10.7.

Table 6
Testing dataset and the monthly mean of SSN and solar flux F10.7

Month/year	Mean SSN	Mean solar flux F10.7	Solar activity level
May 2008 and April 2009	8.39	71.22	Low
November 2004 and May 2005	44.72	93.00	Medium
October 2011 and January 2012	110.00	146.71	High

2.5.2 Error analysis

The test dataset was used to assess the final output of the BPNN and BPNN–PSO models during the training phase. Not all the test data were included in the training and validation phases. The mean squared error (MSE) was selected to represent the results of the BPNN and BPNN–PSO models. The performance of both models was determined using the root-mean-square error (RMSE), mean absolute error (MAE), mean absolute percentage error (MAPE) and correlation coefficient (R). Eq. (5) was used to calculate RMSE:

$$RMSE = \sqrt{\frac{1}{N}\sum_{i=1}^{n}\left(\overline{f_{obs}} - \overline{f_{pre}}\right)^2} \tag{5}$$

In addition, MAE was determined based on the difference between the measured and predicted f_oF_2 values for the BPNN model. MAE can be calculated as follows:

$$MAE = \frac{1}{N}\sum_{i=1}^{N}\left|f_{pre} - f_{obs}\right|, \tag{6}$$

where f_{pre} is the predicted value of f_oF_2 and f_{obs} represents the measured f_oF_2 from the CADI data. MAPE can be established as follows:

$$MAPE = \frac{1}{N}\sum_{i=1}^{N}\frac{\left|f_{pre} - f_{obs}\right|}{f_{obs}} \times 100\%. \tag{7}$$

3. Results and Discussions

3.1 Testing Result During Low, Medium and High Solar Epoch

Table 7 summarizes the prediction results of the BPNN and BPNN–PSO models for years of low, medium and high solar activity considering more than 4,500 testing data. The forecast results for the output of both models are similar to the findings by Zhao *et al.,* [9], where f_oF_2 was predicted using a neural network with a GA, RMSE ranged from 0.55 MHz to 2.09 MHz and R ranged from 0.73 to 0.94. The research conducted by Zheng *et al.,* [1] yielded an RMSE between 0.54 MHz and 1.47 MHz, whilst R was between 0.82 and 0.92.

Table 7
Daily test results for low, medium and high solar activities using the BPNN and BPNN–PSO models

Solar activity level	Model	MAPE (%)	RMSE (MHz)
Low solar activity	BPNN	6.94	0.58
	BPNN–PSO	5.27	0.50
Medium solar activity	BPNN	5.60	0.49
	BPNN–PSO	4.16	0.32
High solar activity	BPNN	4.38	0.41
	BPNN–PSO	2.48	0.24

The average RMSE for the BPNN and BPNN–PSO models during low, medium and high solar activities ranged from 0.24 MHz to 0.58 MHz, while the average MAPE was from 2.48% to 6.94%. R was between 0.88 and 0.94. RMSE and MAPE were better for the BPNN–PSO model compared with the performance of the BPNN model. The RMSE for the BPNN–PSO model was from 0.24 MHz to 0.50 MHz. The MAPE values ranged from 2.48% to 5.27%. The BPNN–PSO model outperformed the BPNN model, exhibiting lower RMSE and MAPE. These findings were consistent with the results by Fan *et al.,* [2], which stated the BPNN with PSO models provided higher predictive accuracy than the only BPNN model. In all three scenarios of low, medium and high solar activity, BPNN–PSO showed better forecasting compared with the BPNN model.

Overall, forecasting during the period of high solar activity provided the lowest average predictive error of 2.48% using the BPNN–PSO model. This outcome could be due to the fact that during this period, even though the solar activity level was high, the geomagnetic activities were mostly quiet with only a few weak storms. However, despite having a large amount of low solar activity data during the training phase, the outcome of the testing phase for low solar activity testing data achieved a forecasting error of 5.27% for the BPNN–PSO model, which was relatively high compared with high and medium solar activity.

Few cases are presented here representing the condition of low, medium and high solar activity in Figure 6 to Figure 8. Figure 6 compares the actual f_oF_2 and the models' predictions during low solar activity and quiet geomagnetic activity. During low solar years, the BPNN–PSO model produced higher predictive output than the BPNN model, in which the average RMSE and MAPE were 0.50 MHz and 5.27%, respectively. Overall, the BPNN–PSO model outperformed the BPNN model. The prediction of each model followed the trend of the actual value. However, the BPNN–PSO forecast was marginally accurate at most data points due to the optimum data selection using PSO algorithm prior to the training phase.

For example, on 7 May 2008, when the D_{st} and equivalent K_p indices were −14 nT and 7, respectively (i.e., quiet condition), the prediction error of the BPNN–PSO model was 1.02%, resulting f_oF_2 of 6.78 MHz, which was closer to the actual value of 6.85 MHz compared with the prediction of the BPNN model, which was 5.49% higher than the actual value. These results indicated that a low error percentage made the BPNN–PSO model more accurate than the BPNN model. Similarly, on 20 April 2009 with D_{st} and equivalent K_p indices of −2 nT and 17, respectively, the prediction error of the BPNN–PSO model was only 0.39% (f_oF_2= 7.64 MHz), which was closer to the actual value of f_oF_2

(i.e., 7.61 MHz). The BPNN model underpredicted the actual value of f_oF_2 with 7.01 MHz, which was 7.88% lower than the actual value.

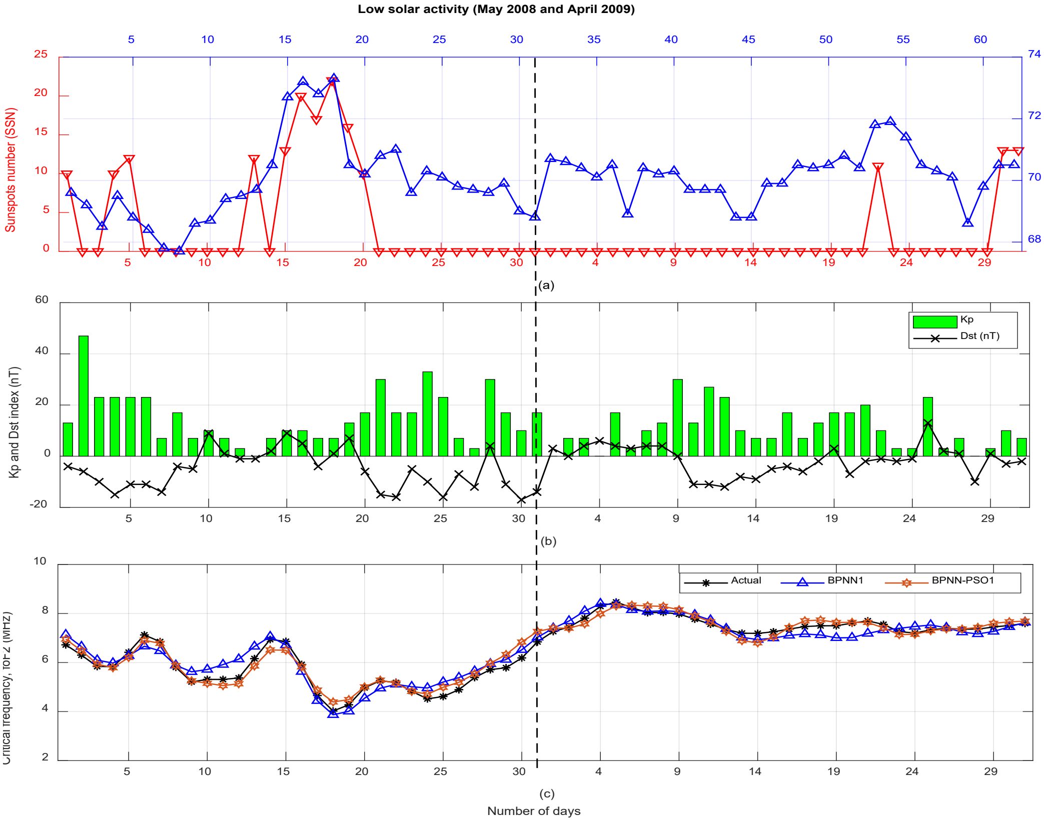

Fig. 6. Comparison of actual f_oF_2 and the models' predictions during low solar activity (May 2008 and April 2009): (a) daily SSN and solar flux F10.7 (b) D_{st} and equivalent K_p indices (c) actual (black), BPNN (orange) and BPNN–PSO (blue)

Figure 7 illustrates the performance of the BPNN and BPNN–PSO models during medium solar activity. Despite the occurrence of geomagnetic storms on 8 November 2004, both models fit the rising and falling segments of the f_oF_2 curve well during medium solar activity, as shown in Figure 7(c). The BPNN–PSO model achieved lower prediction error between the actual and predicted values than the BPNN model.

For example, on 8 November 2004, the values of D_{st} and equivalent K_p were −343 nT and 83 (K_p= 8^+), respectively, which can be considered an intense storm. The prediction of the BPNN–PSO model was 4.42 MHz, which was 0.94% closer to the actual value, that is, 4.38 MHz. Simultaneously, the BPNN model was 12.36% higher than the actual value (3.84 MHz). In addition, on 10 November 2004, the BPNN–PSO model demonstrated its capability to predict accurately during another occurrence of geomagnetic storm. On that day, the values of D_{st} and equivalent K_p were −135 nT and 77 (K_p= 8^-), respectively, which meant an intense storm. The prediction of the BPNN–PSO model was 2.44 MHz and the actual f_oF_2 was 2.11 MHz.

Furthermore, on 15 May 2005, the BPNN–PSO model demonstrated its capability to predict accurately during the occurrence of geomagnetic storm. The values of D_{st} and equivalent K_p were −105 nT and 53 (K_p= 5^+), respectively, suggesting an intense storm. The prediction of the BPNN–PSO model was 1.59% (7.65 MHz), which was closer to the actual f_oF_2 of 7.53 MHz. The prediction of the BPNN model was overestimated because it was 4.59% (7.87 MHz) higher than the actual value. Figure 7(c) shows the BPNN model could not match the actual f_oF_2 values during these two months. Overall, these results indicated the BPNN–PSO forecast outperformed that of the BPNN model, even when geomagnetic storms occurred during medium solar activity.

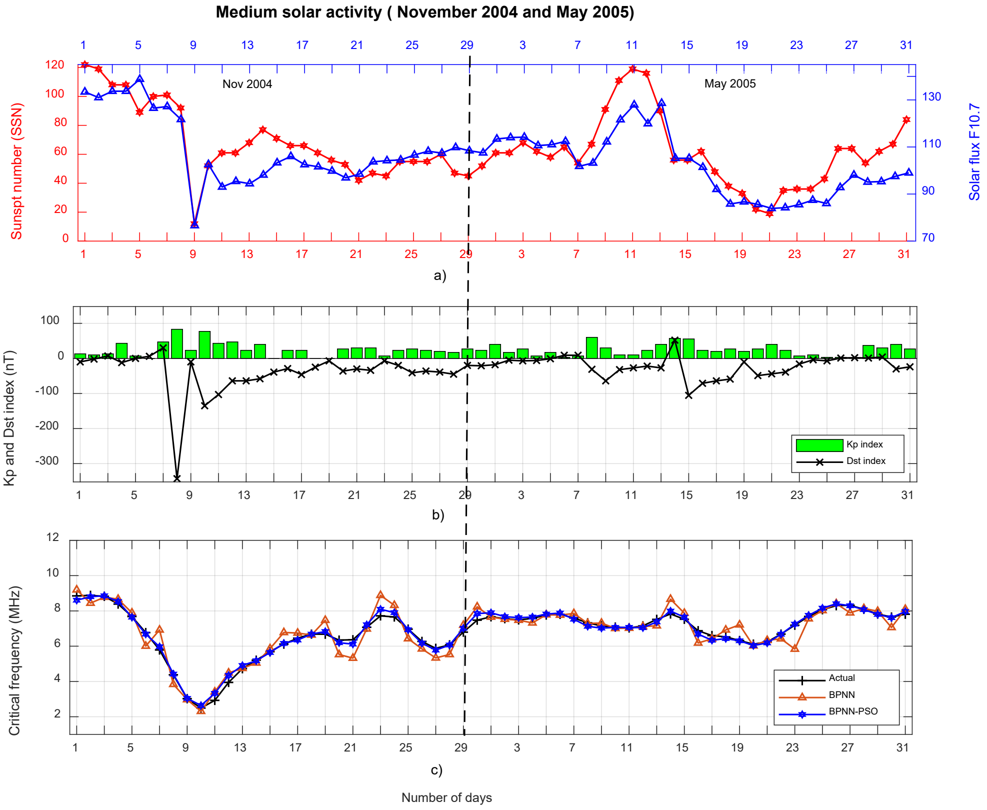

Fig. 7. Comparison of actual f_oF_2 and the models' predictions during medium solar activity (November 2004 and May 2005): (a) daily SSN and solar flux F10.7 (b) D_{st} and equivalent K_p indices (c) actual (black), BPNN (orange), (red) and BPNN–PSO (blue)

The BPNN–PSO model also performed better than the BPNN model during high solar activity. The average RMSE of the BPNN–PSO model was 0.24 MHz and its average MAPE was 2.48%. Figure 8 compares the actual f_oF_2 and the models' predictions during high solar activity, with solar and geomagnetic activity values.

On 23 January 2012, D_{st} and equivalent K_p were −62 nT and 23 (K_p= 2^+), respectively. The BPNN–PSO forecast was 5.68 MHz (MAPE= 1.39%), which was closer to the actual f_oF_2 value of 5.76 MHz. By contrast, the BPNN model slightly underpredicted the actual value of f_oF_2 at 1.91% error, forecasting an f_oF_2 of 5.65 MHz. These observations revealed the BPNN–PSO forecast was apparently more accurate than that of BPNN during high solar activity with moderate storms.

On 25 October 2011, the D_{st} and equivalent K_p values were −40 nT and 17 (K_p= 2^-), respectively, signifying a weak storm. The BPNN–PSO prediction was more accurate in terms of percentage error, which was only 0.52%, forecasting an f_oF_2 of 7.67 MHz. The BPNN model was 2.98% (7.48 MHz) below the actual value of f_oF_2, that is, 7.71 MHz. The BPNN–PSO model can provide accurate predictions under quiet and disturbed geomagnetic conditions at high solar activity because it achieved lower prediction error at most data points.

The BPNN–PSO model performed better than the BPNN model. These findings agree with the results by Zhao *et al.,* [9], which concluded that the BPNN model with optimization methods, such as PSO and GA, can reasonably predict f_oF_2, with only a slight error ranging from 0.13 MHz to 0.42 MHz.

Based on the findings when the BPNN–PSO model was used, the predicted and actual values of f_oF_2 were comparable under quiet and geomagnetic storm conditions. Our BPNN–PSO worked very well in forecasting the critical frequency of the F2 layer, even in high solar activity and achieved the best outcome during this period. However, the testing data mostly covered quiet and weak geomagnetic conditions.

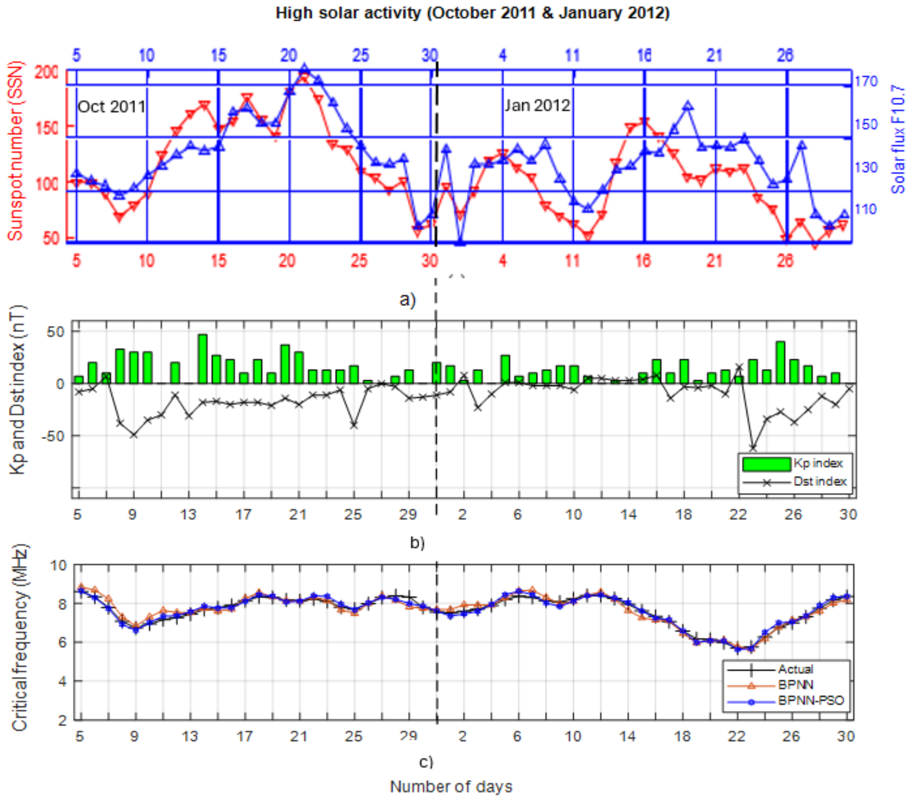

Fig. 8. Comparison of actual f_oF_2 and the models' predictions during high solar activity (October 2011 and January 2012): (a) daily SSN and solar flux F10.7 (b) D_{st} and equivalent K_p indices (c) actual (black), BPNN (orange) and BPNN–PSO (blue)

4. Conclusions

All the tests were performed using the BPNN and BPNN–PSO models. The test results were analysed in terms of MAPE and RMSE. Two datasets, namely, the monthly and diurnal test data, were used to perform the test phase. Data from May 2008, April 2009, November 2004, May 2005, October 2011 and January 2012 were used to represent low, medium and high solar activity data. The BPNN–PSO model, with RMSE and MAPE equal to 0.50 MHz and 5.27%, respectively, during low solar activity, performed the best.

The BPNN–PSO model performed better than the BPNN model during medium solar activity, achieving the lowest RMSE and MAPE of 0.32 MHz and 4.16%, respectively. Moreover, the best model for high solar activity was the BPNN–PSO model, with 0.24 MHz and 2.48% RMSE and MAPE, respectively. Overall, the performance of the BPNN–PSO model was better than that of the BPNN model during low, medium and high solar activities. In addition, the BPNN–PSO model performed the best, particularly during high solar activity, because it exhibited the lowest RMSE and MAPE.

The proposed work can be further expanded by adjusting the weight and bias of the PSO algorithm during training to improve the performance accuracy of the prediction model, particularly under disturbed conditions. Furthermore, different training methods, such as the Elman neural network, can be used to build an f_oF_2 prediction model to determine whether different training methods can yield more reliable results than previous ones.

Acknowledgment

This work was supported by the Universiti Tun Hussein Onn Malaysia under GPPS Vot No. H569. The authors thank J.H. King and N. Popitoshvili at ONET, NASA GSFC and Cawed for providing the index data.

References

[1] Zheng, Dunyong, Wusheng Hu and Peiqing Li. "Predicting ionospheric critical frequency of the F2 layer over Lycksele using the neural network improved by error compensation technology." *Survey Review* 48, no. 347 (2016): 130-139. https://doi.org/10.1179/1752270615Y.0000000015

[2] Fan, Jieqing, Chao Liu, Yajing Lv, Jing Han and Jian Wang. "A short-term forecast model of foF2 based on Elman neural network." *Applied Sciences* 9, no. 14 (2019): 2782. https://doi.org/10.3390/app9142782

[3] Ezquer, R. G., M. A. Cabrera, J. L. Lopez, M. R. Albornoz, M. Mosert, P. Marco and D. Buresova. "Critical frequency and maximum electron density of F2 region over four stations in the North American sector." *Journal of atmospheric and solar-terrestrial physics* 73, no. 4 (2011): 420-429. https://doi.org/10.1016/j.jastp.2010.09.018

[4] Wang, Jinlong, Guoru Ding and Haichao Wang. "HF communications: Past, present and future." *China Communications* 15, no. 9 (2018): 1-9. https://doi.org/10.1109/CC.2018.8456447

[5] Pietrella, M. "A short-term ionospheric forecasting empirical regional model (IFERM) to predict the critical frequency of the F2 layer during moderate, disturbed and very disturbed geomagnetic conditions over the European area." In *Annales Geophysicae*, vol. 30, no. 2, pp. 343-355. Göttingen, Germany: Copernicus Publications, 2012. https://doi.org/10.5194/angeo-30-343-2012

[6] Wichaipanich, Noraset, Kornyanat Hozumi, Pornchai Supnithi and Takuya Tsugawa. "A comparison of neural network-based predictions of foF2 with the IRI-2012 model at conjugate points in Southeast Asia." *Advances in Space Research* 59, no. 12 (2017): 2934-2950. https://doi.org/10.1016/j.asr.2017.03.023

[7] Nakamura, Maho I., Takashi Maruyama and Yasunari Shidama. "Using a neural network to make operational forecasts of ionospheric variations and storms at Kokubunji, Japan." *Earth, planets and space* 59 (2007): 1231-1239. https://doi.org/10.1186/BF03352071

[8] Oyeyemi, E. Oㅒ and L. A. McKinnell. "A new global F2 peak electron density model for the International Reference Ionosphere (IRI)." *Advances in space research* 42, no. 4 (2008): 645-658. https://doi.org/10.1016/j.asr.2007.10.031

[9] Zhao, Jun, Xiaojun Li, Yi Liu, Xiang Wang and Chen Zhou. "Ionospheric foF2 disturbance forecast using neural network improved by a genetic algorithm." *Advances in Space Research* 63, no. 12 (2019): 4003-4014. https://doi.org/10.1016/j.asr.2019.02.038

[10] Athieno, Racheal, P. T. Jayachandran and D. R. Themens. "A neural network-based foF2 model for a single station in the polar cap." *Radio Science* 52, no. 6 (2017): 784-796. https://doi.org/10.1002/2016RS006192

[11] Jiang, Chunhua, Chen Zhou, Jing Liu, Ting Lan, Guobin Yang, Zhengyu Zhao, Peng Zhu, Hengqing Sun and Xiao Cui. "Comparison of the Kriging and neural network methods for modeling foF2 maps over North China region." *Advances in Space Research* 56, no. 1 (2015): 38-46. https://doi.org/10.1016/j.asr.2015.03.042

[12] Salimov, B. G., O. I. Berngardt, A. E. Khmelnov, K. G. Ratovsky and O. A. Kusonsky. "Application of convolution neural networks for critical frequency foF2 prediction." *Solar-Terrestrial Physics* 9, no. 1 (2023): 56-67. https://doi.org/10.12737/stp-91202307

[13] Armaghani, D. Jahed, M. Hajihassani, E. Tonnizam Mohamad, A. Marto and S. A. Noorani. "Blasting-induced flyrock and ground vibration prediction through an expert artificial neural network based on particle swarm optimization." *Arabian Journal of Geosciences* 7 (2014): 5383-5396. https://doi.org/10.1007/s12517-013-1174-0

[14] Xie, Kun, Hong Yi, Gangyi Hu, Leixin Li and Zeyang Fan. "Short-term power load forecasting based on Elman neural network with particle swarm optimization." *Neurocomputing* 416 (2020): 136-142. https://doi.org/10.1016/j.neucom.2019.02.063

[15] Zhao, Xiukuan, Baiqi Ning, Libo Liu and Gangbing Song. "A prediction model of short-term ionospheric foF2 based on AdaBoost." *Advances in Space Research* 53, no. 3 (2014): 387-394. https://doi.org/10.1016/j.asr.2013.12.001

[16] Wang, Jian, Hongmei Bai, Xiangdong Huang, Yuebin Cao, Qiang Chen and Jianguo Ma. "Simplified regional prediction model of long-term trend for critical frequency of ionospheric F2 Region over east Asia." *Applied Sciences* 9, no. 16 (2019): 3219. https://doi.org/10.3390/app9163219

[17] Chen, C., Z. S. Wu, Z. W. Xu, S. J. Sun, Z. H. Ding and P. P. Ban. "Forecasting the local ionospheric foF2 parameter 1 hour ahead during disturbed geomagnetic conditions." *Journal of Geophysical Research: Space Physics* 115, no. A11 (2010). https://doi.org/10.1029/2010JA015529

[18] Atulkar, Roshni, Shivangi Bhardwaj, Prakash Khatarkar, Purushottam Bhawre and P. K. Purohit. "Geomagnetic disturbances and its impact on ionospheric critical frequency (foF2) at high, mid and low latitude region." *American Journal of Astronomy and Astrophysics* 2, no. 6 (2014): 61-65. https://doi.org/10.11648/j.ajaa.20140206.11

[19] Wang, X., J. K. Shi, G. J. Wang, G. A. Zherebtsov and O. M. Pirog. "Responses of ionospheric foF2 to geomagnetic activities in Hainan." *Advances in Space Research* 41, no. 4 (2008): 556-561. https://doi.org/10.1016/j.asr.2007.04.097

[20] Timoçin, Erdinç, Ali Yeşil and İbrahim Ünal. "The effect of the geomagnetic activity to the hourly variations of ionospheric foF2 values at low latitudes." *Arabian Journal of Geosciences* 7 (2014): 4437-4442. https://doi.org/10.1007/s12517-013-1108-x

[21] Kovalick, T. *SPDF-Coordinated Data Analysis Web (CDAWeb). NASA*. 2004.